J. Phys.: Condens. Matter **9** (1997) 10065–10078. Printed in the UK PII: S0953-8984(97)86579-4

X-ray absorption spectroscopy and molecular dynamics studies of Zn^{2+} hydration in aqueous solutions

A Kuzmin†, S Obst‡ and J Purans†

† Institute of Solid State Physics, Kengaraga Str. 8, LV-1063 Riga, Latvia

‡ Institut für Kristallographie, Freie Universität Berlin, Takustrasse 6, 14195 Berlin, Germany

Received 4 August 1997, in final form 30 September 1997

Abstract. The hydration of Zn^{2+} ions in aqueous solutions was studied at room temperature by x-ray absorption spectroscopy and molecular dynamics (MD) simulation. The extended x-ray absorption fine structure (EXAFS) above the Zn K-edge was interpreted using the multiple-scattering approach by taking into account only one coordination shell composed of 6 ± 0.2 water molecules at R(Zn–O) $= 2.06 \pm 0.02$ Å with a mean square relative displacement (MSRD) $\sigma^2 = 0.009 \pm 0.002$ Å^2. No evidence of significant contributions from the second hydration shell to the EXAFS signal was found in the solutions. This is explained by the cancellation interference effect between double-scattering and single-scattering EXAFS signals in the second shell due to large thermal/static disorder ($\sigma^2 \sim 0.1$ Å^2) as predicted by our MD simulation and by known results of diffraction techniques.

1. Introduction

X-ray absorption spectroscopy offers the unique opportunity to probe the local coordination of ions in solutions. Whereas pair correlation functions can also be obtained by x-ray or neutron diffraction, the extended x-ray absorption fine structure (EXAFS), measured at the absorption edge of an atom, gives information about high-order correlation functions [1, 2]. The presence of such contributions appears in EXAFS as multiple-scattering (MS) effects whose interpretation requires extensive simulations based on modern computational methods [3–5]. The quantitative analysis of EXAFS allows one to obtain a set of structural parameters, as coordination numbers, interatomic distances, mean square relative displacements (MSRD) and bond angles, describing the short range order in the vicinity of the absorbing atom [6].

A number of articles has been published in the past on EXAFS studies on the hydration of 3d-transition metals (see [7–10] for a review). The experimental EXAFS signals, measured at the K-edges of 3d ions in solutions, consist of a dominant low-frequency signal, caused by atoms located in the first coordination shell, and a weak high-frequency signal, attributed either to multiple-scattering effects [11, 12] or to the second hydration shell [13–15]. Thus, it is of great interest to understand the origin of the high frequency signal observed in EXAFS of hydrated ions and its relation with the MS signal and/or the outer shell.

The presence of a second hydration shell around some ions in aqueous solutions has been previously studied and confirmed by x-ray diffraction (XRD) [7, 10]. Among the series of 3d elements, zinc is a promising candidate for such a study because its second

0953-8984/97/4610065+14$19.50

hydration shell in water is well established by XRD [16–19] and was also observed by Monte Carlo simulations [20]. A well ordered second shell, consisting of ∼8–13 water molecules located around the Zn^{2+} ions at a mean distance $R(\mathrm{Zn–OH_2})$ =4.21–4.26 Å with MSRD σ^2 =0.06–0.16 $\mathrm{Å}^2$, was found in 0.6–3.1 M aqueous solutions of $ZnSO_4$ [16]. In addition, the expected regular octahedral coordination of zinc ions [7, 10] simplifies the EXAFS analysis allowing us to concentrate on the high-frequency contribution mentioned before. To our knowledge, relatively few investigations [15, 21–23] have been devoted to EXAFS studies of hydrated zinc ions. The first three studies [21–23] dealt with the first coordination shell only. In the most recent study [15], an attempt was made to interpret the complete EXAFS signal by taking into account both first and second hydration shells.

In the present work, the experimental K-edge EXAFS spectra of Zn^{2+} in aqueous solutions will be analysed using the multiple-scattering formalism, and compared with the EXAFS signals calculated using the zinc-oxygen radial distribution function (RDF) from molecular dynamics (MD) simulations and published XRD data [16, 17]. We will show that in the case of the zinc ion, the experimental EXAFS signal can be well interpreted by taking into account only the first coordination shell, and by attributing the high-frequency component to the MS contribution originating within it. The absence of any significant contribution from the second hydration shell in the EXAFS data is explained by the cancellation interference effect between MS and single-scattering signals generated within the second shell in the presence of strong thermal/structural disorder.

2. Experimental details

Aqueous solutions containing 0.063, 0.125 and 0.25 M Zn^{2+}, were prepared by dissolving appropriate quantities of polycrystalline $ZnSO_4 \cdot 7H_2O$ salt in distillated water. Solid polycrystalline $ZnSO_4 \cdot 7H_2O$ and ZnO powders were used as reference compounds. For x-ray measurements, the solutions were placed in plastic cells with two Mylar windows, whereas the solid powders were finely ground and placed between two Scotch films.

X-ray absorption spectra (XAS) were measured at room temperature in transmission mode at the ADONE storage ring (Frascati, Italy) using the EXAFS station at the PWA BX2S beam line. The storage ring ADONE was operated at 1.5 GeV with current I =30–40 mA. The synchrotron radiation was monochromatized using a Si(220) ($2d$ = 3.84 Å) channel-cut crystal monochromator, and its intensity was measured by two ionization chambers filled with krypton gas. The experimental spectra were recorded in the energy range 9500–10500 eV at the Zn K-edge (E_K = 9658.6 eV) with an energy resolution of ∼2 eV. The total thickness x of all samples was optimized to result in an absorption jump $\Delta\mu x \simeq 1$ (where μ is the absorption coefficient). The experimental XAS of all aqueous solutions were found to be identical within the range of error of the experiment. Hence, only the data for the 0.125 M solution will be discussed in the following as an example.

3. EXAFS data analysis

The experimental XAS were treated by the EXAFS data analysis software package 'EDA' [24] following the standard procedure [25].

For each sample, the x-ray absorption coefficient $\mu(E) = \ln(I_0/I)$ was calculated from the intensities of the synchrotron radiation, measured by two ionization chambers, before (I_0) and after (I) the sample. The background contribution $\mu_b(E)$ was approximated by a Victoreen-like polynomial ($\mu_b = A + B/E^3$) and subtracted from the experimental spectra

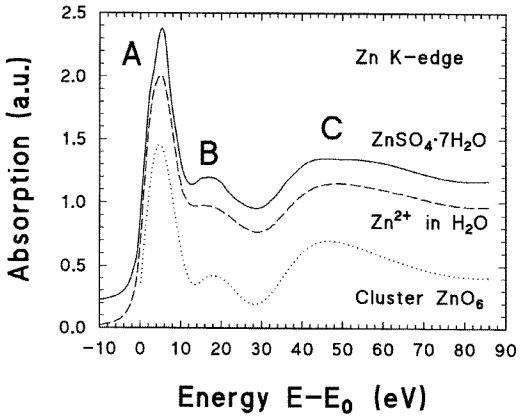

Figure 1. X-ray absorption spectra (XANES region) of the Zn K-edge measured in solid crystalline $ZnSO_4 \cdot 7H_2O$ (solid line) and in an 0.125 M aqueous solution of $ZnSO_4$ (dashed line) in comparison with the calculated signal (dotted line) corresponding to a regular ZnO_6 octahedron with R(Zn–O) = 2.06 Å. Three main features are labelled by the letters A, B and C.

$\mu(E)$. The resulting absorption coefficient in the vicinity of the edge is shown in figure 1. The EXAFS signal $\chi(k)$ was determined as $\chi(k) = (\mu - \mu_b - \mu_0)/\mu_0$ where the atomic-like contribution μ_0 was found by a combined polynomial/cubic-spline technique to allow a precise subtraction of the EXAFS signal baseline. The photoelectron wave vector k was defined as $k = \sqrt{(2m/\hbar^2)(E - E_0)}$, where the energy origin E_0 was located at the absorption edge as shown in figure 1 to get the same energy scale for the experimental and theoretical EXAFS spectra. The experimental EXAFS spectra of the solid crystalline $ZnSO_4 \cdot 7H_2O$ and its 0.125 M aqueous solution are compared in figure 2(a) (upper curves). Note that they are essentially identical except for a small difference in the amplitude of oscillations at low k-values.

The Fourier transforms (FTs) of the EXAFS $\chi(k)k^2$ signals, multiplied by a Kaiser–Bessel window with the parameter $A = 2$ [24], were calculated in the k-range 0.5–13 $Å^{-1}$ (figure 2(b)). Note that the positions of peaks in the FTs differ from the true crystallographic values by a quantity of the photoelectron phase shifts (about 0.46 Å for the first peak). The EXAFS contributions from the first coordination shell (see middle curves in figure 2(a)), composed of oxygen atoms, were singled out by a back-FT procedure in the R-range 0.5–2.2 Å (figure 2(b)).

It is clearly evident in figure 2(b) that a group of similar peaks is present beyond the first shell for both solid crystalline $ZnSO_4 \cdot 7H_2O$ and its 0.125 M aqueous solution. Due to the small intensity of these peaks (compared to the first shell signal), they were extracted by subtracting the first shell EXAFS signal from the experimental signal (see lower curves in figure 2(a)). In this way, the possible influence of the FT procedure on the EXAFS signal from the distant low-intense peaks was minimized.

The first shell EXAFS $\chi(k)k^2$ signals in the range 1.5–12 $Å^{-1}$ were utilized in the best-fit analysis procedure, assuming the single-shell Gaussian model

$$\chi(k) = S_0^2 N \frac{f(\pi, k, R)}{kR^2} \exp(-2\sigma^2 k^2) \sin(2kR + \phi(\pi, k, R)). \tag{1}$$

Thus, a set of three structural parameters (N, the coordination number; R, the interatomic

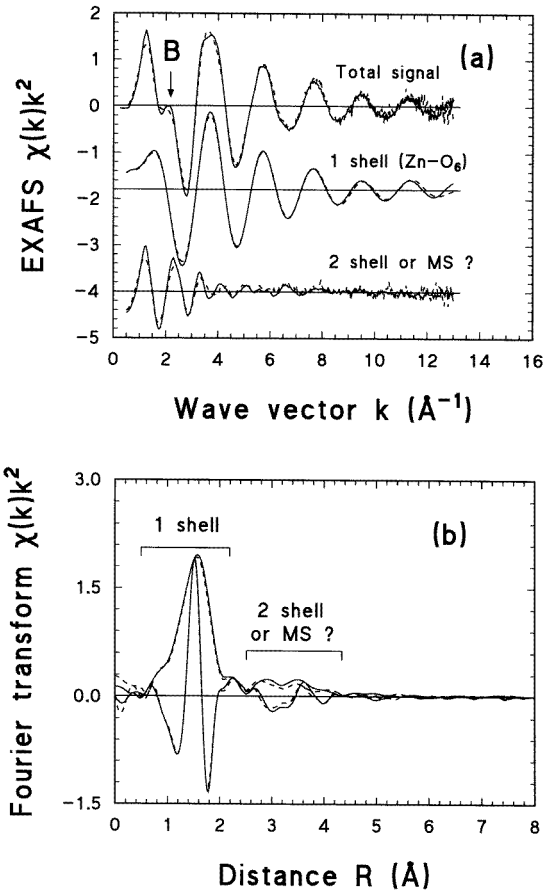

Figure 2. (a) The experimental EXAFS-signals $\chi(k)k^2$ of the Zn K-edge measured in solid crystalline $ZnSO_4 \cdot 7H_2O$ (solid curves) and in an 0.125 M aqueous solution of $ZnSO_4$ (dashed curves). The total EXAFS signals (upper curves) and the contributions from two regions indicated in (b) are shown. (b) Fourier transforms of the experimental EXAFS-signals $\chi(k)k^2$ shown in (a). Two main regions (the first shell and the high-frequency signal contribution originating from the second shell or from MS) are indicated.

Zn–O distance; σ^2, the mean square relative displacement (MSRD)) was obtained for each sample. The value of S_0^2, the EXAFS amplitude reduction factor due to multi-electron processes, was determined by setting the value of N for $ZnSO_4 \cdot 7H_2O$ to 6 and was fixed for both ZnO and aqueous solution. The scattering amplitude $f(\pi, k, R)$ and phase $\phi(\pi, k, R)$ functions were calculated using the *ab initio* FEFF6 program [26]. The calculations were performed for a cluster with a radius of 8 Å having the structure of $ZnSO_4 \cdot 7H_2O$ [27] and centred at the Zn atom. The EXAFS amplitude damping, related to the inelastic mean-free path of the photoelectron and to the Zn K-edge core-hole lifetime, taken from [28], was included automatically in the scattering amplitude function by the use of the complex Hedin–Lundqvist exchange and correlation potential [26]. Because the experimental Zn K-edge EXAFS signals of the aqueous solution and crystalline $ZnSO_4 \cdot 7H_2O$ are similar

(see figure 2), we assumed that the described model can be used for the calculation of $f(\pi, k, R)$ and $\phi(\pi, k, R)$ values for the aqueous solutions.

The results of the fits for the first shell EXAFS signals are presented in table 1 and in figure 3(b). Note that the number of free parameters (N, R and σ^2), used in the fits, was significantly smaller than the number of independent data points defined as $N_{ind} \approx 2\Delta k \Delta R/\pi \sim 11$ where Δk and ΔR are the ranges of the EXAFS signal in k and R space [32].

Table 1. Structural data for the first coordination shell of zinc in aqueous solutions and reference crystals. (N is the coordination number, R is the interatomic distance and σ^2 is the MSRD.)

Method	N	R(Zn–O) (Å)	σ^2 (Å^2)
	ZnO crystal		
EXAFS (this work)	4±0.2	1.98±0.02	0.004±0.002
ND [38]	4	1.978	
	$ZnSO_4 \cdot 7H_2O$ crystal		
EXAFS (this work)	6	2.06±0.02	0.008±0.002
XRD [27]	2	1.96	
	2	2.03	
	2	2.11	
	Zn^{2+}–ions in aqueous solutions		
EXAFS (this work)	6±0.2	2.06±0.02	0.009±0.002
MD (this work)	6	2.08	0.0028
EXAFS [15]	6	2.05	0.0096
EXAFS [21]	6	2.12	0.008
EXAFS [22]	6	2.07	0.0066
EXAFS [23]	6	2.07	0.0065
XRD [16]	6	2.13	0.010
XRD [17]	6	2.11	0.010
XRD [18]	6	2.074	0.025
XRD [19]	6	2.10	0.026
XRD [29]	6.2	2.09	
XRD [30]	6	2.08	
ND [31]	5.3	2.09	0.0169
Ab initio MO calculations [39]	6	2.04	
Ab initio MO calculations [40]	6	2.12	
MC simulations [20]	6	2.05	

4. Multiple-scattering calculations

To understand the origin of the peaks in the FT spectra beyond the first shell, we consider two structural models, for which the EXAFS signals were calculated by the *ab initio* multiple-scattering FEFF6 program [26].

The first model was the regular ZnO_6 cluster with R(Zn–O) = 2.06 Å (given by EXAFS). The calculated multiple-scattering (MS) paths and related EXAFS signals, which produce the largest contribution, are presented in figure 4. The total EXAFS signal for the ZnO_6 cluster is shown by a dotted line in figure 1 (the XANES part) and by a thick solid line in figure 3(a) (the EXAFS part). Note that the sum of the DS1, DS2, TS1 and TS4 signals is responsible for the origin of the feature B in figures 1 and 2(a). The features A and C in figure 1 are mainly due to the single-scattering by six oxygen atoms of the first shell.

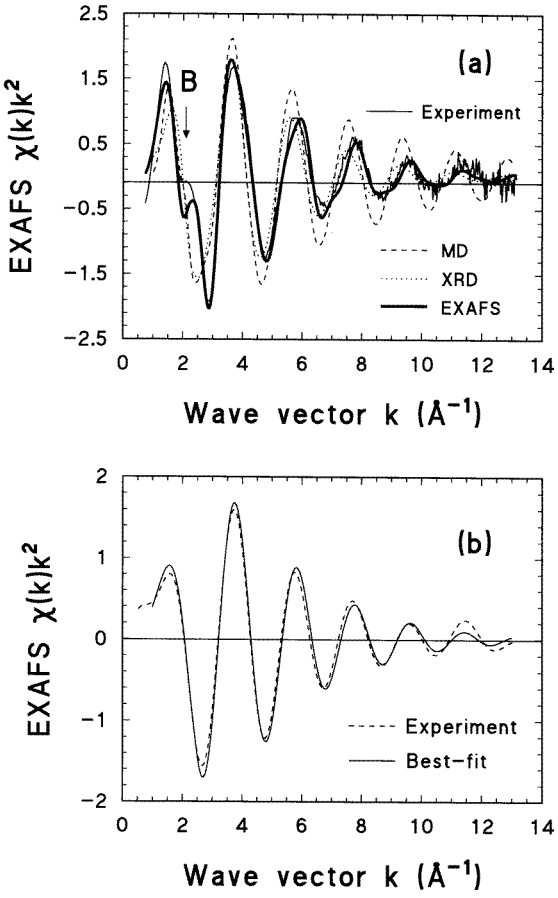

Figure 3. Comparison of the experimental EXAFS signals of the Zn K-edge in the 0.125 M aqueous solution of $ZnSO_4$ with the results of the EXAFS analysis, the MD simulation and a model based on XRD data from [16, 17]. (a) Total EXAFS signals. The position of the feature B (cf. figure 1) is indicated. The total EXAFS model equal to the sum of signals in (b) and (c) is shown by a thick solid line. Obviously, MD (dashed curve) and XRD (dotted curve) models result in higher frequencies as compared to the experiment (thin solid line) and are not able to reproduce feature B. Additionally, the EXAFS signal based on the MD model is less damped than the other signals due to the extremely narrow peak of the radial distribution function distribution for the first hydration shell (cf. (d)). (b) The first shell experimental (dashed lines) and best-fit (solid lines) EXAFS signals for $ZnSO_4 \cdot 7H_2O$, Zn^{2+} in aqueous solution and ZnO (see table 1 for the values of structural parameters). The calculations were performed using the single-scattering single-shell Gaussian approximation. (c) Comparison between EXAFS spectra calculated using different methods and models for the explanation of the high frequency experimental EXAFS signal. The MD (dashed curve) and XRD (dotted curve) models were calculated in the single-scattering approximation from the respective parts ($R > 3$ Å) of the RDFs (see (d)), assuming the origin of the high frequency EXAFS signal to be due to the outer hydration shells of zinc. The EXAFS model is based on the assumption of the first shell multiple-scattering (MS) origin of the high frequency signal. (d) The radial distribution functions (RDFs) $G_{Zn-O}(R)$ obtained by EXAFS (dashed line), XRD (dotted line) (according to [16, 17]) and MD (solid line). Note that no second-shell contribution is detected by EXAFS (see figure 5 for explanation).

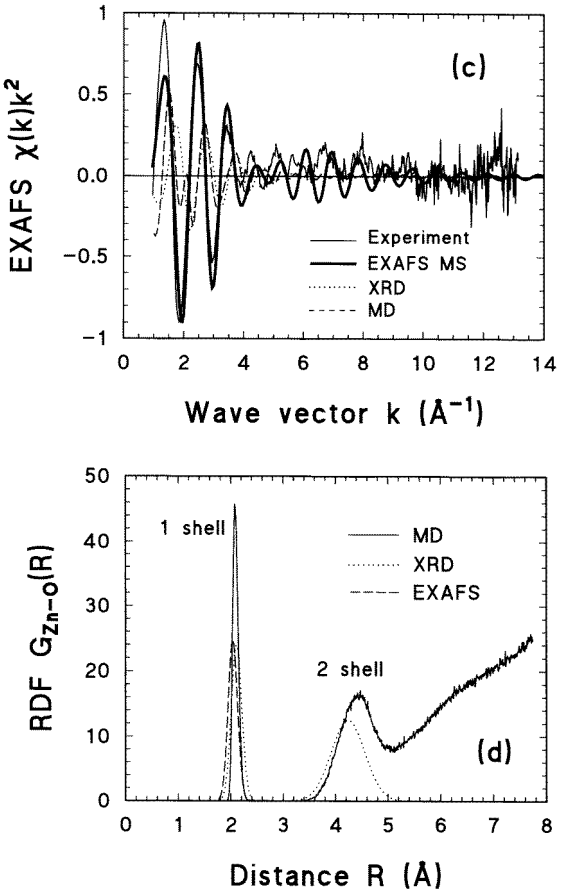

Figure 3. (Continued)

The second model was a three atom chain Zn–O_1–O_2 (where O_i denotes the oxygen atom in the ith coordination shell) with the angle $\widehat{ZnO_1O_2} = 124^\circ$ (from MD simulations (see section 5)) and the distances R(Zn–O_1) = 2.06 Å (given by EXAFS) and R(Zn–O_2) = 4.24 Å (given by XRD). This model was used to check the importance of the contribution from the MS signals versus the contribution from the second hydration shell found by XRD [16–19]. Among several MS signals generated within the chain, the DS signal, shown in figure 5, has its frequency close to that of the SS signal from the second shell, and they therefore contribute to the same region in R-space. Comparing the SS and DS signals in the absence of thermal damping (the upper curves in figure 5), one observes that they are strongly different at high k-values (>4 $Å^{-1}$), however, at low k-values (<4 $Å^{-1}$) the two signals are out of phase with comparable amplitudes. After thermal damping was included by multiplying both signals with the Debye–Waller factor $\exp(-2\sigma^2k^2)$ with σ^2 = 0.1 $Å^2$ (the value suggested for the second shell by XRD [16, 17] and MD (see section 5)), the two signals became similar except for the phase, so that their sum was expected to be close to zero leading to the cancellation of the second shell contribution to the total EXAFS signal.

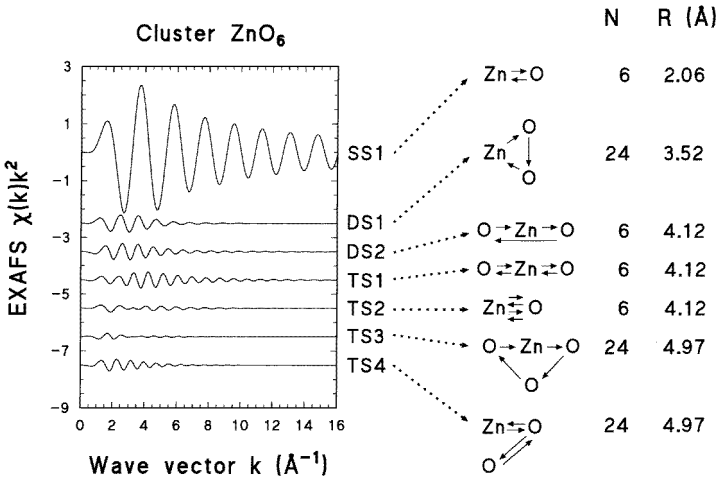

Figure 4. The most important multiple-scattering (MS) EXAFS signals generated within the ZnO_6 cluster. N is the path degeneracy (equal to the coordination number for the single-scattering path SS1) and R is the half-path length (equal to the Zn–O interatomic distance for the path SS1). Among high-order MS signals, the double-scattering DS1 and DS2 signals and the tripple-scattering TS1 and TS4 signals are the largest ones and, moreover, they are in-phase at low k-values, being responsible for the origin of the feature B in figures 1 and 3(a).

5. Molecular dynamics simulation

Molecular dynamics (MD) simulations were performed on SGI workstations (Silicon Graphics) in the same way as described in [33, 34] using the program CHARMM [35] with the CHARMM22 force field as provided by MSI (Molecular Simulations Inc., Waltham, MA, USA). The system consisted of a Zn^{2+} ion surrounded by 123 molecules of water in a cubic box of 15.5 Å side length with periodic boundary conditions (i.e. central box plus 26 images). Water was represented by the TIP3P model [36], and standard parameters from CHARMM22 were used for the Zn^{2+} ion. The time step for integration by the leapfrog-algorithm was 1 fs. Information about energies and temperature variations during the simulation is given in table 2. More details on the MD simulation can be found in [33, 34].

Table 2. Values of times (in ps), energies (in kcal mol^{-1}) and temperatures T (in K) for the MD simulation. (SD is the standard deviation.)

	Time	E_{kin}±SD	E_{pot}±SD	E_{tot}±SD	T±SD
Min	20.10	181.8	−1762.5	−1518.8	247.9
Max	1064.70	255.6	−1593.1	−1402.6	348.5
Average		219.8±9.3	−1668.3±47.0	−1448.5±46.0	299.8±12.7

The simulation was performed in three steps: during the first 10 ps the system was heated from 0 to 300 K, after that, it was equilibrated at 300 K for 10 ps and, finally, the coordinate sets were collected during the next 1000 ps at a time interval of 0.1 ps. Using these coordinate sets, the Zn–O radial distribution function (RDF) $G_{Zn-O}(R)$ (solid line in figure 3(d)) and the $Zn–O_{1st\ shell}–O_{2nd\ shell}$ angle distribution were calculated. The

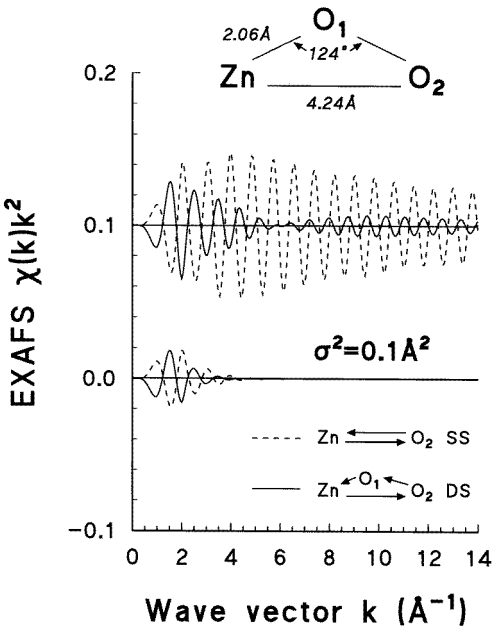

Figure 5. Results of the MS calculations for a three-atom system Zn–O_1–O_2 with $\widehat{ZnO_1O_2} = 124^\circ$. The dashed line represents the single-scattering (SS) by the oxygen atom O_2 of the second shell, the solid line corresponds to the double-scattering (DS) contribution involving the oxygen atoms O_1 of the first and O_2 of the second shell. The two upper curves do not account for any damping whereas the lower curves were multiplied by the Debye–Waller factor $\exp(-2\sigma^2k^2)$ with $\sigma^2 = 0.1$ Å^2. The σ^2-value for the second shell is derived from XRD [16, 17] and MD.

values of the $Zn–O_{1st\ shell}–O_{2nd\ shell}$ angle are subject to a slightly asymmetric Gaussian-like distribution with the maximum located at 124° and the FWHM being equal to ∼35°. The obtained structural parameters for the first and second hydration shells of zinc are given in tables 1 and 3, respectively.

Table 3. Structural data for the second hydration shell of zinc in aqueous solutions. (N is the coordination number, R is the interatomic distance and σ^2 is the MSRD.)

Method	*N*	*R*(Zn–O) (Å^2)	
MD (this work)	∼ 14	4.39	0.12
XRD [16]	7.6–13.2	4.21–4.26	0.058–0.16
XRD [17]	9.9	4.24	0.078
XRD [18]	12	4.25	0.109
XRD [19]	6	4.26	0.14
EXAFS [15]	11.6±1.6	4.1±0.2	0.039±0.009
MC simulations [20]	16–18	4.20	

To compare the results of the MD simulation with the experimental EXAFS data, the $\chi(k)$ signal was calculated from the RDF $G_{Zn-O}(R)$ according to [37]

$$\chi(k) = \int_0^{+\infty} G_{Zn-O}(R)\frac{f(\pi, k, R)}{kR^2}\sin(2kR + \phi(\pi, k, R))\mathrm{d}R$$

$$= \int_0^{+\infty} G_{\mathrm{Zn-O}}(R)\gamma(R,k)\mathrm{d}R. \tag{2}$$

Here, the meaning of all parameters is the same as in equation (1). As mentioned before [37], due to the short range nature of the Kernel $\gamma(R,k)$, the integral in (2) can be numerically evaluated by introduction of a maximum distance cut-off $R_{\mathrm{cut-off}}$. Care has been taken to avoid termination ripples [37] when $G_{\mathrm{Zn-O}}(R)$ was truncated at $R_{\mathrm{cut-off}} = 7.5$ Å. The calculated EXAFS signal is shown in figure 3(a), and the contribution from $G_{\mathrm{Zn-O}}(R)$ at long distances ($R > 3$ Å) is presented in figure 3(c).

6. Results and discussion

Before discussing the results for the aqueous solutions of Zn^{2+}, we will briefly consider data obtained for two reference compounds. This will provide the reader with an estimate of the reliability of the structural parameters for the first shell of zinc.

The first reference compound is zinc oxide: it has a wurtzite-type structure where each atom is surrounded by a tetrahedron of atoms of the other element. The structural parameters of ZnO were precisely determined by neutron diffraction (ND) [38]: the first shell around a zinc atom consists of four oxygen atoms located at the mean distance of 1.978 Å (there are three Zn–O distances equal to 1.9747 Å and one Zn–O distance equal to 1.9886 Å). This value of the Zn–O distance is in excellent agreement with the one determined by EXAFS (see table 1). Note that a small static disorder within the first shell of zinc allows one to consider the value of the MSRD $\sigma^2 = 0.004$ Å^2 to be mainly due to thermal vibrations.

The second reference compound, zinc sulphate heptahydrate $ZnSO_4 \cdot 7H_2O$, has a structure composed of $Zn(H_2O)_6$ octahedra and SO_4 tetrahedra with the extra H_2O molecules located in empty spaces [27]. The distance between a zinc atom and its surrounding water molecules varies between 1.95 and 2.14 Å: there are six different distances equal to 1.959, 1.960, 2×2.029, 2.083 and 2.134 Å, which were grouped in table 1 into three subshells with mean distances equal to 1.96, 2.03 and 2.11 Å. The outer shells of zinc form a broad distribution: there are 16 oxygen atoms located between 2.8 and 4.7 Å with the mean distance $\sim$ 3.99 Å and the mean square deviation $\sigma^2 = 0.157$ Å^2. The shortest distance between the absorber and two nearest zinc atoms is $\sim$ 4.71 Å. The broad distribution of atoms in the outer shells of zinc leads to a very small contribution of these atoms to the total EXAFS signal. As a result, the experimental EXAFS signal of the crystalline $ZnSO_4 \cdot 7H_2O$ (solid lines in figures 1 and 2) is similar to the spectra of zinc in aqueous solutions. The only visible difference between them is a slightly larger broadening of the XANES in the solution (figure 1). The best-fit results for the first shell in $ZnSO_4 \cdot 7H_2O$ are compared with the XRD data [27] in table 1. Note that the MSRD value $\sigma^2 = 0.008$ Å^2 of the Zn–O bond reflects both static σ^2_{st} and thermal σ^2_{th} disorder. By taking the value of $\sigma^2_{\mathrm{th}} = 0.004$ Å^2 (as in ZnO), one gets $\sigma^2_{\mathrm{st}} = \sigma^2 - \sigma^2_{\mathrm{th}} = 0.004$ Å^2 being in excellent agreement with a static disorder of 0.004 Å^2 due to a distribution of distances as suggested by XRD.

Finally, we conclude that the good agreement between our results and the ones derived by ND [38] for ZnO and by XRD [27] for crystalline $ZnSO_4 \cdot 7H_2O$ reflects the reliability of the calculated scattering amplitude and phase functions.

The best fit of the first shell of zinc in aqueous solution is shown in figure 3(b). The obtained values of structural parameters are presented in table 1. The zinc ions are coordinated by six molecules of water at 2.06 Å with $\sigma^2 = 0.008$ Å^2. The coordination number agrees well with the one found in our MD simulation and in other experimental [15–19, 21–23, 29, 30] and theoretical [20, 39, 40] studies. The value of the MSRD is

consistent with other EXAFS [15, 21–23] and some XRD [17, 21] studies. It should be noted that a much lower value of the MSRD was obtained in our MD simulations leading to the narrow first shell peak in the RDF (solid line in figure 3(d)) and to smaller damping of the EXAFS signal (dashed line in figure 3(a)). This difference in MSRD between MD and EXAFS/XRD is probably related to the simplicity of the Lennard-Jones-potential function used for the calculation of nonbonded interactions in the MD simulation.

The mean Zn–O distance 2.06 Å agrees well with the previoulsy reported EXAFS results [15, 22, 23]. On the other hand, it is about 0.04 Å shorter than the average value determined by XRD and ND (table 1) (a distribution of R(Zn–O) values ranging from 2.08 to 2.13 Å has been suggested by diffraction studies with 2.10 Å being the mean value). The Zn–O distance of 2.08 Å given by MD simulation is defined by the potential parameters, which were chosen to be in agreement with XRD results. Since the interatomic distance is related to the frequency of the EXAFS signal (see equation (1)), it can be determined with high accuracy when the backscattering phase function $\phi(\pi, k, R)$ is reliably known. In this work, $\phi(\pi, k, R)$ was tested on two reference crystalline compounds leading to very good agreement with known structural data. We therefore consider the value of R(Zn–O) = 2.06 Å to be sufficiently accurate, and we used it in the MS calculations for ZnO_6 and Zn–O_1–O_2 clusters (figures 4 and 5, respectively).

Thus, for the first hydration shell of zinc all experimental methods produce comparable results. However, the question about the existence of the second hydration shell and its contribution to the experimental EXAFS signal still remains open.

Our MD simulation suggests the presence of a second shell formed by ∼14 water molecules at 4.39 Å with $\sigma^2 = 0.12$ Å^2. The coordination number and the MSRD agree well with the average values provided by XRD studies [16, 17, 18]. The position of the second peak (cf figure 3(d)) is found 0.14 Å farther away from the zinc ion than suggested by XRD (4.24 Å). Note that the latter value was used in the MS EXAFS calculation for the Zn–O_1–O_2 cluster (figure 5). Thus, the existence of the second hydration shell around zinc ions in aqueous solutions is well established, but two questions remain: 'Is it possible to observe the second shell contribution in the EXAFS?' and 'What is the origin of the high-frequency signal, whose contribution is well visible in both the XANES (feature B in figure 1) and the EXAFS (figure 2) parts of the experimental signal?'

As mentioned before, up to now no common point of view has been established as to whether the high-frequency signal present in the EXAFS spectra of 3d-ions in solutions is caused by MS effects [11, 12] or by the second hydration shell [13–15]. To our knowledge, there is only one previous work [15] on the Zn K-edge EXAFS in aqueous solutions where the question of the contribution of the second hydration shell of Zn^{2+} was risen. The authors of [15] criticized the interpretation based on the MS model and attributed the signal to the second hydration shell composed of 11.6 ± 1.6 molecules of water located at 4.1 ± 0.2 Å with a MSRD $\sigma^2 = 0.039 \pm 0.009$ Å^2. However, no MS calculations were presented in [15]. Besides, the obtained distance and MSRD values differ from the ones provided by XRD (cf table 1). From our point of view, the analysis performed in [15] in the k-space interval from 3.1 to 11.7 Å^{-1}, where the contribution of the high-frequency signal is very small compared to the first shell signal, just occasionally resulted in the set of structural parameters looking close to the XRD ones. Moreover, to get a reasonable accuracy of the fit, the authors varied the inner potential correction ΔE_0, so that the difference between the ΔE_0 values for the first and second shells was as much as 2.2–5.4 eV (see table 3 in [15]). It is well known [6] that the variation of ΔE_0 leads to additional errors in interatomic distances by modifying the phase of the EXAFS signal. We are convinced that the ΔE_0 correction was necessary to compensate a difference in the phases of the second shell single-scattering and the first

shell multiple-scattering EXAFS contributions and, thus, to attain an agreement with the experimental data.

For the sake of clarity, we are going to discuss our results for several models, which support the interpretation of the high-frequency signal as resulting from the MS contribution generated within the first shell. In addition, we will show that the contribution of the second hydration shell to the EXAFS signal is negligible due to the cancellation interference effect between scattering signals.

We used three models to simulate the EXAFS signal for zinc in solution. The first model is represented by the ZnO_6 cluster discussed in section 4. The second model is based on the results of the MD simulation and was described in section 5. The third model is based on the average XRD data. For these three models, the total EXAFS signal and the contribution from the MS or the second hydration shell were calculated as described in sections 4 and 5 and are compared with the experimental data in figures 3(a) and 3(c). As can be seen in figure 3(a), the first model gives the best agreement and, moreover, it is the only model which reproduces feature B of the experimental data. From close comparison of the high-frequency contributions for the three models with the experimental data shown in figure 3(c), obviously only the first model is in agreement with the frequency and the amplitude of the experimental signal. The other two models suggest lower frequencies and significantly reduced amplitudes. Note that no fitting parameter was used in the calculation of all three models. Hence, we conclude that the origin of the high-frequency contribution is due to the MS effects in the first coordination shell of zinc. Additionally, we would like to point out that, as shown before [41], the multiple-scattering contribution generated within the first shell of the octahedrally coordinated ions is significant in the k-space range up to $6-7$ Å^{-1} for any atom in the Periodic Table. This is due to a number of linear atom chains present in the octahedron. Moreover, the MS signals are less sensitive to the distortion of the octahedron than the single-scattering signals [41]. Therefore, MS contributions can be also expected in other solutions where the cation is coordinated by six water molecules.

However, the interesting question remains: 'Why is the second shell contribution not visible in the EXAFS despite its amplitude being supposedly quite high?' The answer can be found in the model calculations for the Zn–O_1–O_2 cluster as discussed in section 4. In figure 5, the single-scattering (SS) and double-scattering (DS) signals generated within the Zn–O_1–O_2 chain are shown. When no disorder is present ($\sigma^2 = 0$), the amplitude of the SS signal is significantly higher than the amplitude of the DS signal especially at high values of k (see upper curves in figure 5). However, in the presence of disorder ($\sigma^2 = 0.01$ Å^2) similar to the one expected for the second shell from XRD data, both signals show amplitudes which are comparable in magnitude but opposite in phase (see lower curves in figure 5). As a result, the sum of the two signals tends to be close to zero and, hence, the second shell contribution is not visible in the experimental EXAFS spectrum. We would like to point out that this result is not in contradiction to the existence of a second hydration shell in the vicinity of zinc ions in aqueous solutions, but shows that the second shell contribution can be strongly damped in EXAFS, due to cancellation interference effect with other multiple-scattering signals, and therefore care should be taken when EXAFS signals for ions in solutions are interpreted.

The cancellation interference effect observed in the present case is not unique and has been observed before in other compounds. For example, such an effect is responsible for the strong damping of the second shell signal in crystalline silicon resulting in the much lower value of the coordination number compared to the crystallographic one [42]. One should point out that the origin of the effect is related to (i) the particular geometric configuration (relative position) and (ii) the scattering amplitude and phase functions of atoms participating

in the scattering process. Therefore, this effect can be in principle present in any EXAFS signal, and the accurate multiple-scattering calculations give the only straightforward check for the case of a particular system.

7. Conclusions

The x-ray absorption spectroscopy study of the hydration of Zn^{2+} ions in 0.063, 0.125 and 0.25 M aqueous solutions of $ZnSO_4 \cdot 7H_2O$ has been performed at the Zn K-edge. No difference in the EXAFS signals was observed for different concentrations confirming previous results [15]. The zinc ion is coordinated by six molecules of water located at 2.06 ± 0.02 Å with the MSRD $\sigma^2 = 0.009 \pm 0.002$ Å^2. It was shown that the XANES and the total EXAFS signals can be interpreted best by considering only one coordination shell for the zinc ion. The high-frequency contribution present in both XANES and EXAFS parts was attributed to the multiple-scattering signals generated within the first shell. The absence of a second hydration shell contribution was explained by the cancellation interference effect between single-scattering and double-scattering signals generated within the $Zn–O_1–O_2$ atom chains (O_i denotes the oxygen atom in the ith coordination shell).

Acknowledgments

Two of us (AK and JP) would like to thank Professor E Burattini and the staff of the PWA laboratory (INFN, LNF, Frascati) for the opportunity to carry out experiments at the PWA-BX2S beam line. This work was partially supported by the Latvian Government research grants 93.652 and 96.0670.

References

[1] Rehr J J, Albers R C and Zabinsky S I 1992 *Phys. Rev. Lett.* **69** 3397
[2] Tyson T A, Hodgson K O, Natoli C R and Benfatto M 1992 *Phys. Rev.* B **46** 5997
[3] Binsted N, Gurman S J, Campbell J W and Stephenson P 1982 *EXCURVE. Daresbury Laboratory Program, 1982* (CCLRC Daresbury Laboratory, Warrington WA4 4AD, Cheshire, UK)
[4] Mustre de Leon J, Yacoby Y, Stern E A, Rehr J J and Dell'ariccia M 1989 *Physica* B **158** 263
[5] Filipponi A, Di Cicco A, Tyson T A and Natoli C R 1991 *Solid State Commun.* **78** 265
[6] Teo B K 1986 *EXAFS: Basic Principles and Data Analysis* (Berlin: Springer)
[7] Ohtaki H and Radnai T 1993 *Chem. Rev.* **93** 1157
[8] Neilson G W and Enderby J E 1989 *Adv. Inorg. Chem* **34** 195
[9] Marcus Y 1988 *Chem. Rev.* **88** 1475
[10] Magini M, Licheri G, Pashina G, Piccaluga G and Pinna G 1988 *X-Ray Diffraction of Ions in Aqueous Solutions: Hydration and Complex Formation* (Boca Raton, FL: Chemical Rubber Company Press)
[11] Garcia J, Bianconi A, Benfatto M and Natoli C R 1986 *J. Physique* **47** C8-49
[12] Garcia J, Sanchez del Rio M, Burattini E, Benfatto M and Natoli C R 1989 *Physica* B **158** 409
[13] Sandstrom D R, Dodgen H W and Lytle F W 1977 *J. Chem. Phys.* **67** 473
[14] Sandstrom D R and Lytle F W 1979 *Ann. Rev. Phys. Chem.* **30** 215
[15] Muñoz-Páez A, Pappalardo R R and Sanchez Marcos E 1995 *J. Am. Chem. Soc.* **117** 11710
[16] Licheri G, Paschina G, Piccaluga G and Pinna G 1982 *Z. Naturf.* A **37** 1205
[17] Musinu A, Paschina G, Piccaluga G and Magini M 1982 *J. Appl. Cryst.* **15** 621
[18] Caminiti R, Cucca P, Monduzzi M, Saba G and Crisponi G 1984 *J. Chem. Phys.* **81** 543
[19] Radnai T, Palinkas G and Caminiti R 1982 *Z. Naturf.* A **37** 1247
[20] Yongyai Y P, Kokpol S and Rode B M 1991 *Chem. Phys.* **156** 403
[21] Miyanaga T, Watanabe I and Ikeda S 1988 *Chem. Lett.* 1073
Sakane H, Miyanaga T, Watanabe I and Yokoyama Y 1990 *Chem. Lett.* 1623
Miyanaga T, Sakane H, Watanabe I and Ikeda S 1992 *Photon Factory Activity Report* (Tsukuba: National Laboratory for High Energy Physics) p 167

[22] Funahashi S, Inada Y and Ozutsumi K 1992 *Photon Factory Activity Report* (Tsukuba: National Laboratory for High Energy Physics) p 251
[23] Ozutsumi K, Yamaguchi T, Ohtaki H, Tohji K and Udagawa Y 1985 *Bull. Chem. Soc. Japan* **58** 2786
[24] Kuzmin A 1995 *Physica* B **208&209** 175
1996 *EDA: EXAFS Data Analysis Software Package User's Manual* (available from the author)
1997 *J. Physique IV* **7** C2-213
[25] Kuzmin A, Mironova N, Purans J and Rodionov A 1995 *J. Phys.: Condens. Matter* **7** 9357
Kuzmin A, Mironova N and Purans J 1997 *J. Phys.: Condens. Matter* **9** 5277
[26] Rehr J J , Mustre de Leon J, Zabinsky S I and Albers R C 1991 *J. Am. Chem. Soc.* **113** 5135
Mustre de Leon J, Rehr J J, Zabinsky S I and Albers R C 1991 *Phys. Rev.* B **44** 4146
[27] Wyckoff R W G 1963 *Crystal Structures* vol 3 (New York: Wiley) p 839
[28] Keski-Rahkonen O and Krause M O 1974 *At. Data Nucl. Data Tables* **14** 139
[29] Bol W, Gerrits G J A and van Eck C L Van P 1970 *J. Appl. Cryst.* **3** 486
[30] Ohtaki H, Yamaguchi T and Maeda M 1976 *Bull. Chem. Soc. Japan* **49** 701
[31] Powell D H, Gullidge P M N, Neilson G W and Bellissent-Funel M C 1990 *Mol. Phys.* **71** 1107
[32] Report on the International Workshop on Standards and Criteria in XAFS 1991 *Proc. 6th Int. Conf. on X-ray Absorption Fine Structure (York)* ed S S Hasnain (Singapore: Ellis Horwood) p 751
[33] Obst S and Bradaczek H 1996 *J. Phys. Chem.* **100** 15677
[34] Obst S and Bradaczek H 1997 *J. Mol. Model.* **3** 224
[35] Brooks B R, Bruccoleri R E, Olafson B D, States D J, Swaminathan S and Karplus M 1983 *J. Comput. Chem.* **4** 187
[36] Jorgensen W L, Chandrasekhar J, Madura J D, Impey R W and Klein M L 1983 *J. Chem. Phys.* **79** 926
[37] Filipponi A 1994 *J. Phys.: Condens. Matter* **6** 8415
[38] Kisi E H and Elcombe M M 1989 *Acta Cryst.* C **45** 1867
Albertsson J, Abrahams S C and Kvick Å 1989 *Acta Cryst.* B **45** 34
[39] Sano M and Yamatera H 1983 *Ions and Molecules in Solution* ed N Tanaka *et al* (Amsterdam: Elsevier) p 109
[40] Bock C W, Kaufman Katz A and Glusker J P 1995 *J. Am. Chem. Soc.* **117** 3754
[41] Kuzmin A and Grisenti R 1994 *Phil. Mag.* **70** 1161
[42] Bianconi A, Di Cicco A, Pavel N V, Benfatto M, Marcelli A, Natoli C R, Pianetta P and Woicik J 1987 *Phys. Rev.* B **36** 6426